MOLECULAR ONCOLOGY 6 (2012) 182–195

available at www.sciencedirect.com

SciVerse ScienceDirect

www.elsevier.com/locate/molonc

Review

Molecular imaging for personalized cancer care

Moritz F. Kircher, Hedvig Hricak, Steven M. Larson*

Department of Radiology, Memorial Sloan-Kettering Cancer Center, 1275 York Avenue, Room C-278, NY 10065, USA

ARTICLE INFO

Article history:
Received 31 October 2011
Received in revised form
20 February 2012
Accepted 20 February 2012
Available online 10 March 2012

Keywords:
Molecular imaging
Oncology
Diagnostics
Theranostics
PET/CT
MRI
MR/PET
PET/MRI
Optical imaging
Raman spectroscopy
Hyperpolarized MRI
MR spectroscopic imaging

ABSTRACT

Molecular imaging is rapidly gaining recognition as a tool with the capacity to improve every facet of cancer care. Molecular imaging in oncology can be defined as *in vivo* characterization and measurement of the key biomolecules and molecularly based events that are fundamental to the malignant state. This article outlines the basic principles of molecular imaging as applied in oncology with both established and emerging techniques. It provides examples of the advantages that current molecular imaging techniques offer for improving clinical cancer care as well as drug development. It also discusses the importance of molecular imaging for the emerging field of theranostics and offers a vision of how molecular imaging may one day be integrated with other diagnostic techniques to dramatically increase the efficiency and effectiveness of cancer care.

1. Introduction

Molecular imaging is rapidly gaining recognition as a tool that has the capacity to improve every facet of cancer care. The growing demand among physicians, patients, and society for personalized care is increasing the importance of molecular imaging and shaping the development of biomedical imaging as a whole. Anatomic imaging will continue to play a role in cancer management, including cancer detection and staging and assessment of treatment response. Applications of anatomical imaging are constantly advancing. For example, in the assessment of tumor response, tumor volume measurement on cross-sectional imaging is being developed and may eventually replace conventional one- or two-dimensional tumor measurement. Over time, biomedical imaging will become more and more multimodal in nature, as different anatomic and molecular imaging techniques can complement each other. Already, positron emission tomography (PET), which is commonly performed with the radiotracer ^{18}F-fluoro-2-deoxy-D-glucose [FDG], is integrated with cross-

* *Corresponding author*. Tel.: +1 212 639 7284; fax: +1 212 794 4010.
E-mail address: hricakh@mskcc.org (H. Hricak).

1574-7891/$ – see front matter © 2012 Federation of European Biochemical Societies. Published by Elsevier B.V. All rights reserved.
doi:10.1016/j.molonc.2012.02.005

sectional imaging in the form of PET/computed tomography (PET/CT). It is inevitable that combined PET/magnetic resonance imaging (MRI)/MR spectroscopic imaging (MRSI), as well as optical imaging, will also play important roles in oncologic imaging in the future. Judging from recent research, it is likely that refined molecular imaging will provide a personalized molecular fingerprint of individual tumors, as a basis for novel treatment algorithms. Furthermore, molecular imaging will facilitate more rapid development of new drugs, including theranostic drugs (i.e., agents that combine diagnostic and therapeutic capabilities).

Molecular imaging in oncology can be defined as *in vivo* characterization and measurement of the key biomolecules and molecularly based events that are fundamental to the malignant state. This definition is deliberately broad, and incorporates both cellular and molecular features of the cancer phenotype. Specifically, molecular imaging interrogates the abnormal molecules as well as the aberrant interactions of altered biomolecules that are the basis for neoplasia. In contrast, "classical" diagnostic imaging primarily images the advanced manifestation of cancer.

This article outlines the basic principles of molecular imaging as applied with both established and emerging techniques. It then provides specific examples of the advantages that current molecular imaging techniques offer for improving each step of clinical cancer care as well as drug development. Finally, it discusses the importance of molecular imaging for the emerging field of theranostics and offers a vision of how molecular imaging may one day be integrated with other diagnostic techniques to dramatically increase the efficiency and effectiveness of cancer care.

2. Principles of molecular imaging in oncology

Although molecular imaging has existed for decades, recent, rapid advances in molecular and cell biology, imaging technology, and imaging probe development have greatly increased its power and potential. Essential to the development and translation of molecular imaging is interdisciplinary collaboration across many fields, including radiology, nuclear medicine, pharmacology, chemistry, molecular and cell biology, physics, mathematics, and engineering. An array of sophisticated molecular imaging technologies are now available for use in preclinical and clinical settings (Bradbury and Hricak, 2005; Grassi et al., 2008; Kircher et al., 2011; Kircher and Willmann, in press-a, in press-b; Weissleder and Pittet, 2008; Zavaleta et al., 2011). These include positron emission tomography (PET), single photon emission computed tomography (SPECT), computed tomography (CT), MRI, MRSI, ultrasound, and optical imaging (Kircher et al., 2011; Kircher and Willmann, in press-a, in press-b; Weissleder and Pittet, 2008).

Molecular imaging can be achieved using either endogenous information or exogenous probes. MRSI and certain optical techniques are examples of molecular imaging using endogenous information. MRSI combines the ability of spectroscopy to acquire a large volume of metabolic information, with the ability of imaging to localize information spatially. Although phosphorus (^{31}P) and carbon (^{13}C) MRSI are possible, proton (^{1}H) MRSI is the technique most often used in clinical settings. On ^{1}H MRSI tumor spectra contain resonances from taurine, total choline (choline, phosphocholine, and glycerophosphocholine), total creatine (phosphocreatine and creatine), and lactate (Howe et al., 1993); generally, tumors exhibit elevated choline and lactate levels (W.N, 1992). Novel optical imaging techniques such as intrinsic Raman spectroscopy can also achieve molecular imaging by using endogenous information. Raman spectroscopy is based on detection of photons that have changed their wavelength after interaction with specific atomic bonds in molecules, and therefore allows elegant characterization of the underlying tissue composition (Zavaleta et al., 2011). The ability of Raman spectroscopy to discriminate malignant from benign tissues has already been demonstrated in a multitude of both preclinical and clinical studies (Zavaleta et al., 2011).

Most molecular imaging approaches, however, rely on the use of exogenous probes to provide imaging signal or contrast. In some cases, the probe may be a conventional contrast agent. For example, with contrast-enhanced (DCE)-MRI, images are acquired sequentially during the passage of an agent such as gadolinium within a tissue of interest. DCE-MRI is not an intrinsically molecular method, but rather provides an indirect assessment of molecular processes that influence blood flow and vascularization (for this reason, it is mentioned here but not described in detail in the section on applications). As changes in tumor vascularity can often be detected earlier than changes in tumor size, DCE-MRI has been used to monitor the early effects of, and predict longer-term responses to, cancer treatments such as anti-angiogenesis drugs, androgen deprivation therapy for prostate cancer, radiotherapy for rectal and cervical cancers, and chemotherapy for bladder and breast cancers (Padhani and Leach, 2005).

The majority of molecular imaging probes have a more sophisticated design and include both a targeting component (e.g. an antibody, peptide, or small molecule) and a signaling component (e.g. a radionuclide for PET or SPECT, a fluorochrome for optical imaging, or a paramagnetic chelate for MRI (Kircher and Willmann, in press-a, in press-b)). Molecular imaging probes can be broadly classified into four categories (Weissleder and Pittet, 2008):

1) *Phenotypic probes* are used to assess general features of malignant physiology, such as metabolic changes secondary to oncogenic activation (Plathow and Weber, 2008), angiogenesis (Cai and Chen, 2008; Cai et al., 2008), cell proliferation (Bading and Shields, 2008; Conti et al., 2008), hypoxia (Everitt et al., 2009; Krohn et al., 2008), apoptosis (Blankenberg, 2008a, 2008b; Strauss et al., 2008), and the expression of certain receptors or antigens in tumor cells (e.g., hormone receptors and peptide receptors) (Mankoff et al., 2008; Peterson et al., 2008).

An example of phenotypic imaging is PET with the radiolabeled glucose analogue ^{18}F-FDG, a marker for the elevated glucose metabolism that occurs in most cancers. Recently, a new type of phenotypic molecular imaging technology has emerged, termed "hyperpolarized MRI". By creating an artificial non-equilibrium of spins, hyperpolarized MRI increases the sensitivity of MRI by a factor of 10,000 or more (Kurhanewicz et al., 2011). This strong signal enhancement

enables imaging of nuclei other than protons (e.g., ^{13}C and ^{15}N) and allows their molecular distribution to be followed *in vivo* and with very short imaging times in the order of seconds (Golman et al., 2003). Such advances can provide real-time insight into tumor metabolism (Kurhanewicz et al., 2011; Brindle et al., 2011; Viale and Aime, 2010). The molecules currently under study – pyruvate, bicarbonate, lactate, and others – are normally present *in vivo*, as they are products of normal intermediary metabolism. Therefore, the contrast agents used in hyperpolarized MRI (hyperpolarized versions of these normal metabolites) are intrinsically very safe for use in humans (Kurhanewicz et al., 2011). Initial results from the first clinical trial, using hyperpolarized [1-^{13}C]pyruvate in prostate cancer, have not shown any adverse effects (Bole, 2010 and John Kurhanewicz, PhD, personal communication).

2) *Targeted probes* are used to image specific biomolecules (e.g., signal transduction proteins or tumor-associated antigens) that are characteristic of a tumor or class of tumors. An example of a targeted probe is the ^{124}iodine-labeled chimeric antibody G250 (^{124}I-cG250) for PET imaging of carbonic anhydrase IX, which is overexpressed in clear-cell renal carcinoma. Some targeted probes are activatable – that is, they are made of molecules or nanoparticles that undergo inducible change. Activatable probes can be used to localize enzymes, signal transducers, and downstream effectors.
3) *Cell-tracking probes* are employed to localize and follow the movement of cells that may be of importance for tumor survival (e.g., cancer cells, vascular endothelium, stromal cells or stem cells). The cells can be labeled directly with tags (e.g., radiotracers, superparamagnetic tags or fluorescent dyes) (Kircher et al., 2003a, 2008; Koch et al., 2003; Swirski et al., 2006; Zhao et al., 2002) or indirectly via the insertion of marker genes (Kircher et al., 2011; Grimm et al., 2007).
4) *Reporter gene probes* are used to monitor the actions of genes in biologic systems *in vivo*. Gene expression imaging has had a revolutionary impact on laboratory study of cancer biology and is likely to play an important role in clinical trials in the future. Some reporter gene probes have already been used to image human cancers.

3. Clinical applications for MI

The imaging modalities that are currently most important in the management of cancer are CT, PET/CT and MRI. While CT continues to be the most utilized modality in cancer care, due to advances in molecular imaging, utilization rates are now growing faster for MRI and PET/CT than for CT. MRI has the advantages of high anatomical and temporal resolution but, in comparison to PET/CT, is still limited in its ability to deliver functional, metabolic and biological information. Emerging techniques such as MRSI and hyperpolarized MRI may allow better retrieval of such information in the future. PET/CT currently remains the most versatile imaging platform in oncology, and therefore this review emphasizes PET/CT more than other molecular imaging modalities. In certain specialized scenarios, such as in endoscopy and during surgery, optical imaging approaches are emerging. While an exhaustive review of molecular imaging applications is not possible in a single article, we aim to highlight in this section those molecular imaging applications that we consider to be most essential or most promising for the current and future practice of oncology.

3.1. *Diagnosis and staging*

3.1.1. *FDG-PET/CT*

PET/CT has changed the diagnostic algorithm in oncology by substantially influencing the management of patients with cancer (Juweid and Cheson, 2006; Juweid et al., 2007; Lardinois et al., 2003; Seam et al., 2007; von Schulthess et al., 2006; Weber, 2006). Among a variety of radiopharmaceuticals for molecular and metabolic imaging with PET, the most relevant biomarker for cancer remains the glucose analog FDG. In contrast to conventional imaging modalities such as CT, ultrasound and MRI (except for specialized sequences mentioned below), which detect tumors based on morphologic alterations, PET detects and characterizes tumors based on molecular alterations. Following intravenous injection, FDG is taken up by tumor cells, similarly to normal glucose. The subsequent conversion of FDG to FDG-6-monophosphate by the intracellular enzyme hexokinase leads to trapping of the metabolite within the tumor cells (Buck et al., 2010).

In the United States, the Centers for Medicare and Medicaid Services reimburse most oncological indications of FDG-PET, such as staging or restaging of lung cancer, breast cancer, colorectal, esophageal and other gastrointestinal cancers, head and neck cancers, lymphoma, and melanoma (Buck et al., 2010). In Europe, reimbursement for PET studies varies between countries, but generally substantially fewer indications are covered. For example, in Germany, so far non-small-cell lung cancer is the only indication that has been approved for reimbursement by the national health care system (Buck et al., 2010).

PET imaging using FDG takes advantage of one of the hallmarks of cancer, namely the Warburg effect: increased glucose metabolism and conversion of glucose carbon to lactate are characteristics of cancer cells as compared to normal cells (Gatenby and Gillies, 2004; Warburg et al., 1927). This increased glucose metabolism in malignancies is mediated via an increased expression and activity of glucose transporters (GluT) in the cell membrane (Macheda et al., 2005) as well as via changes in the glycolytic enzyme expression and activity (Weber, 1977a, 1977b). This alteration in glucose metabolism represents one of the early events in carcinogenesis (Majumder et al., 2004). Indeed, this imaging principle translates into excellent clinical accuracy. For example, prospective studies have reported a sensitivity of 89–100%, a specificity of 69–100% and an accuracy of 89–96% (Bury et al., 1996; Gupta et al., 1998; Patz et al., 2000). Issues with specificity remain, as FDG is also taken up by benign lesions (e.g., in inflammatory processes). PET/CT is also helpful in the localization of tumors in cases where conventional diagnostic methods are unable to localize the primary site (cancer of unknown primary). A recent review provides a more detailed summary of the diagnostic effectiveness of PET/CT in oncology (Fletcher et al., 2008).

Similarly, for tumor staging, PET/CT offers many advantages over conventional imaging strategies. In principle,

staging of almost all malignancies is possible. FDG-PET has high accuracy for staging non-small-cell lung cancer, gastrointestinal tract cancers including colorectal and esophageal cancer, thyroid cancer, head and neck cancer, melanoma and lymphoma (Buck et al., 2010). Changes in therapeutic management in 15%–40% of patients due to findings on PET/CT have been reported (Juweid et al., 2007; Seam et al., 2007; von Schulthess et al., 2006; Pieterman et al., 2000; Sachs and Bilfinger, 2005). Some tumors, such as neuroendocrine cancers, do not exhibit increased glucose uptake and are therefore not as well suited for staging by FDG-PET/CT (Buck et al., 2010).

3.1.2. *Newer PET tracers*

Several new PET tracers are emerging that can improve the accuracy of PET in known areas of weakness of FDG. For example, ^{11}C-choline PET/CT has high sensitivity and specificity for staging and restaging of prostate cancer. ^{68}Ga-DOTATOC is a new tracer for imaging of neuroendocrine tumors (Buck et al., 2010). ^{18}F-fluoro-dihydrotestosterone (FDHT), an anti-androgen receptor tracer, has demonstrated promise in the detection of bone metastases in androgen-sensitive prostate cancer. For example, in a patient with prostate cancer a bone scan, FDG-PET/CT and FDHT-PET/CT were performed within 1 week. A large number of bone metastases as well as lymph node involvement detected with FDHT PET/CT were not detected with either FDG-PET/CT or bone scan, illustrating the great potential value of molecularly targeted PET tracers (Figure 1). Having novel tracers such as FDHT available, and combining them with established tracers such as FDG, opens fascinating new avenues to interrogate tumor biology. We are at the beginning of understanding the heterogeneity of metastatic disease in individual patients, and multi-tracer PET offers a unique opportunity to examine this heterogeneity *in vivo* (Figure 2).

3.1.3. *DW-MRI*

In the clinical setting, diffusion-weighted MRI (DW-MRI) is used to assess the speed of diffusion of water molecules. As most cancer types demonstrate a restricted (slower) diffusion of water molecules compared to healthy tissues, this phenomenon can be used for cancer detection. Whole-body diffusion-weighted imaging (WB-DWI) has now been evaluated in multiple studies as a potential alternative to PET/CT for metastatic lesion detection. While several studies have found WB-DWI to be as accurate as PET/CT (Ohno et al., 2008), some have found WB-DWI to be less specific than PET/CT, resulting in clinically important over-staging in a percentage of patients (van Ufford et al., 2011). Newer DWI techniques, such as computed DWI resulting in higher b-values, could potentially increase diagnostic specificity by improving the suppression of signal from normal tissues that may mimic disease (Blackledge et al., 2011).

3.1.4. *MRSI*

True MR-based molecular imaging strategies that are clinically available include MRSI. Conventional MRI is able to provide high-resolution localization of prostate tumors via their reduced T2 signal in comparison to the surrounding healthy prostate. In patients with moderate and high-risk tumors, staging using the combination of MRSI and MRI has been reported to be of incremental prognostic significance (Westphalen et al., 2008). Information on tumor metabolism provided by endorectal MRI/MRSI may serve as a predictive marker in prostate cancer, as it can be used to identify patients with a high risk of relapse after radical prostatectomy (Zakian et al., 2010). MRSI, however, has limitations for whole-body imaging in part due to its susceptibility to respiratory and bowel motion.

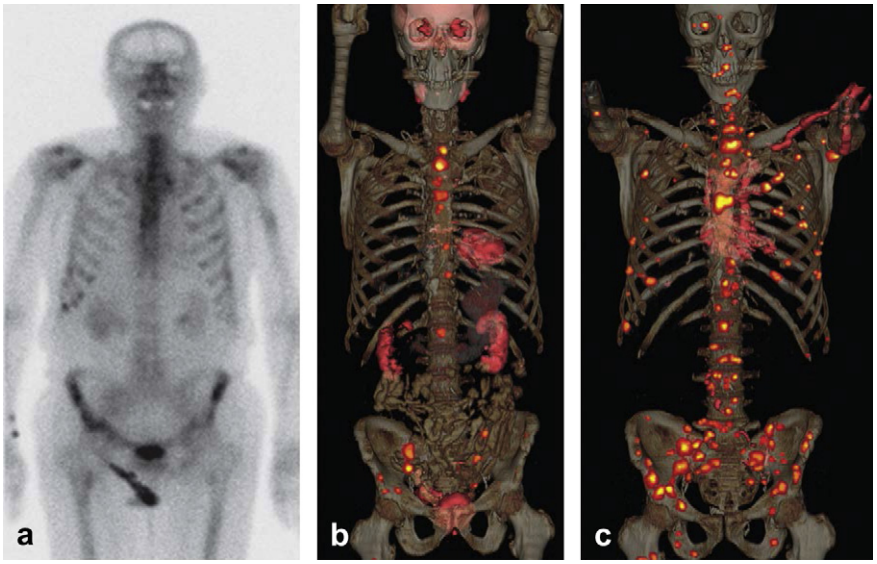

Figure 1 – Images in 79-year-old man with castrate-resistant progressive metastatic prostate cancer (Gleason score, 9; prostate-specific antigen level, 91 ng/mL) who underwent (a) technetium-99 m bone scanning, (b) FDG-PET/CT, and (c) FDHT-PET/CT within the same week. Note the markedly larger number of bone and lymph node metastases demonstrated on c as compared to b or a. Two months after imaging, bone biopsy from the left ilium (the site of suspicious bone metastases demonstrated only on c) showed metastatic disease from primary prostate adenocarcinoma. (Reprinted from Hricak H. Oncologic imaging: a guiding hand of personalized cancer care. Radiology. 2011 Jun; 259(3):633–640).

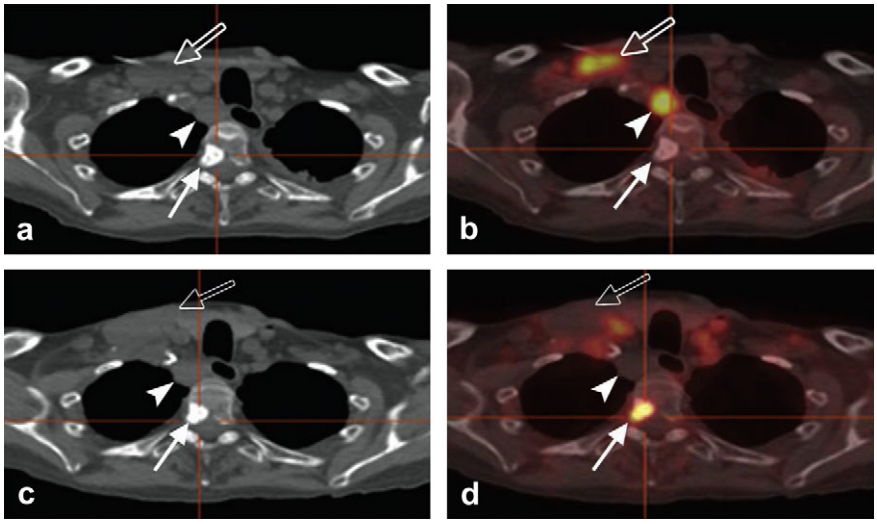

Figure 2 – Images in a 75-year-old man with progressive metastatic prostate cancer starting protocol therapy with abiraterone acetate, an enzyme inhibitor that reduces blood levels of testosterone. (a) CT component of FDG-PET/CT, (b) fused FDG-PET/CT, (c) CT component of FDHT-PET/CT, and (d) fused FDHT-PET/CT images show a sclerotic vertebral lesion (solid arrow) as well as right supraclavicular (open arrow) and retrotracheal (arrowhead) lymphadenopathy. Image b demonstrates increased glycolysis in the retrotracheal and right supraclavicular lymphadenopathy but no uptake in the vertebral bone lesion. Conversely, d demonstrates increased uptake in the vertebral bone lesion but no uptake in the retrotracheal and right supraclavicular lymphadenopathy. Biopsy of the retrotracheal node yielded a finding of "large cell" malignancy, favoring carcinoma, without further classification. This case demonstrates the phenomenon of discordant tumor biology between lesions. (Reprinted from Hricak H. Oncologic imaging: a guiding hand of personalized cancer care. Radiology. 2011 Jun; 259(3):633–640).

3.1.5. *Hyperpolarized MRI*

Hyperpolarized MRI has several key advantages over MRSI, including increased robustness of the resulting imaging data due to very short image acquisition times. Hyperpolarized MRI promises to provide more specific whole-body MRI in the future, as it allows direct insights into metabolic pathways. In preclinical studies it was shown for the first time that tissue pH can be assessed noninvasively via hyperpolarized MRI. Tissue pH is an important parameter, since many pathological states are associated with pH changes. In tumors, for example, the extracellular pH is often lower than in normal tissue and can therefore serve as a biomarker for diagnosis and therapeutic monitoring. According to the Henderson–Hasselbalch equation $(\mathrm{pH} = \mathrm{p}Ka + \log\ ([\mathrm{HCO_3^-}])[\mathrm{CO_2}])$ the local pH can be calculated when both bicarbonate and carbon dioxide concentrations are known (Viale and Aime, 2010; Gallagher et al., 2008). After injection of hyperpolarized ^{13}C-labeled bicarbonate, hyperpolarized carbon dioxide is formed rapidly (through conversion by the enzyme carbonic anhydrase), allowing pH maps of tumors to be created noninvasively (Figure 3) (Gallagher et al., 2008). Given that a wide range of pathologic states including tumors are associated with an acidic environment, whole-body pH mapping could potentially be translated into a generic marker for tumor detection (Kurhanewicz et al., 2011).

3.2. *Treatment guidance*

To date, selection of patients for a particular treatment has generally been based on a variety of patient characteristics but not on mechanisms of resistance. The use of anatomical imaging such as CT or MRI alone to select patients for oncologic therapies, including chemotherapy, radiotherapy, and surgery, is insufficient. Noninvasive and repetitive measurements of biological tumor characteristics have the potential to predict which patients will benefit from a particular treatment and enable more specific patient selection (Bussink et al., 2011; Kaanders et al., 2002; Mandrekar and Sargent, 2010). While FDG-PET/CT is mainly used as a staging tool in current clinical practice, its potential is more far-reaching than that. By providing metabolic information to help select patients and adapt treatment protocols, PET/CT used with FDG and other, more specific PET tracers discussed below promises to enable more personalized cancer care.

3.2.1. *Chemotherapy and biological therapy*

3.2.1.1. *FDG-PET/CT.* In surgically managed lung cancer patients, SUV has been shown to be a predictor of overall survival after resection. The addition of SUVmax to pathologic tumor size can identify a subgroup of patients at highest risk for death from recurrent disease after resection. For example, the 2-year survival for patients with a median SUVmax of more than 9 was 68%, whereas that for patients with a median SUVmax of less than 9 was 96% (Downey et al., 2004).

Treatment outcome could also be predicted with FDG-PET in a phase II trial of 119 patients with esophageal cancer. Patients who exhibited a decrease in SUV $\geq$35% after 2 weeks of chemotherapy were defined as metabolic responders, and patients with an SUV decrease <35% were defined as metabolic nonresponders. The median event-free survival was 29.7 months for metabolic responders but only 14.1 months for nonresponders, and substantial reduction in tumor size was only observed in the responders (Lordick et al., 2007).

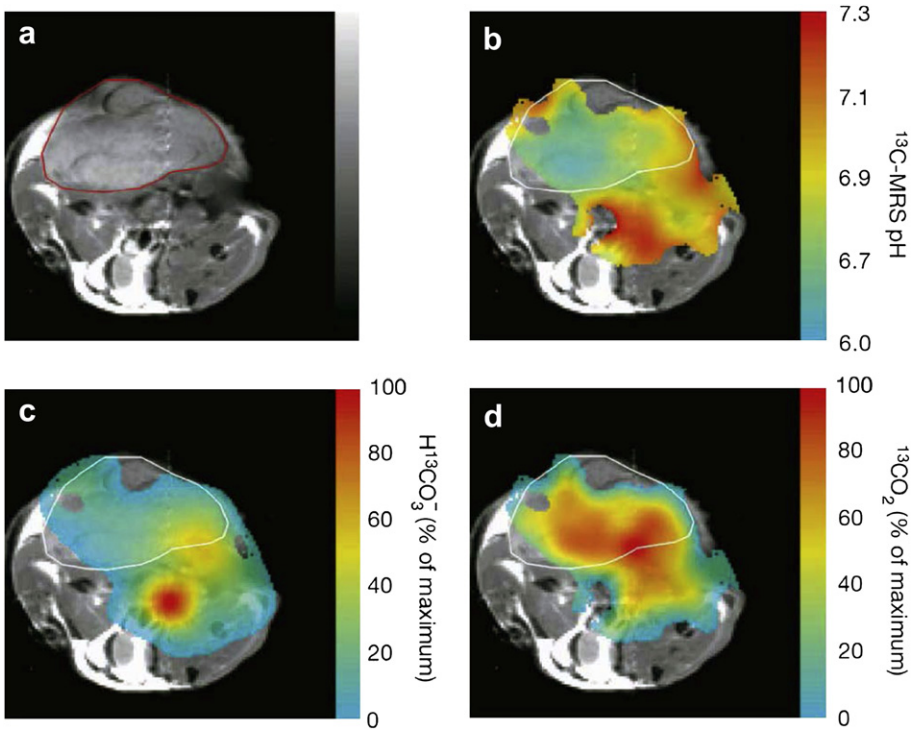

Figure 3 – Imaging of tumor pH *in vivo* using hyperpolarized ^{13}C-labeled bicarbonate. (a) Transverse proton-density weighted spin-echo MR image (TR/TE 1500/30, flip angle, 90°) of a mouse with a subcutaneously implanted EL4 (murine lymphoma) tumor (outlined in red). (b) pH map of the same animal calculated from the ratio of the $H_{13}CO_3^-$ (c) and $^{13}CO_2$ (d) voxel intensities in ^{13}C chemical shift images acquired after intravenous injection of hyperpolarized $H_{13}CO_3^-$. The spatial distribution of $H_{13}CO_3^-$ (c) and $^{13}CO_2$ (d) are displayed as voxel intensities relative to their respective maxima. Tumor margin in b, c and d outlined in white. (Reprinted, with permission, from reference (Gallagher et al., 2008)).

3.2.1.2. *FLT-PET/CT*. In order to measure more specific biological characteristics of tumors, other PET tracers have been developed. These include ^{18}F-3′deoxy-3′-fluorothymidine (FLT), which can measure tumor cell proliferation noninvasively. FLT is retained inside the cell by thymidine kinase 1 and is considered a marker of the S-phase (Rasey et al., 2002; Shields et al., 1998). A key principle advantage of FLT over FDG is that FLT does not exhibit the high physiological uptake in the brain that is seen with FDG, and is therefore better suited for the evaluation of brain neoplasms. For example, in a study examining recurrent high-grade gliomas, SUV changes on FLT-PET scans during biweekly cycles of irinotecan and bevacizumab predicted treatment response. Only those patients who exhibited a significant decrease in SUV during the treatment survived more than 1 year (Schiepers et al., 2010). In patients with non-Hodgkin lymphoma, the SUVs at FLT-PET decreased after only 2 days, and the magnitude of this change predicted whether patients would reach partial or complete responses at the end of their chemotherapy regimen (Herrmann et al., 2007). Similarly, in breast cancer, SUV changes on FLT-PET predicted changes in tumor size early, after 1 week of treatment (Kenny et al., 2007; Pio et al., 2006). FLT-PET has, however, several limitations, such as substantial false-positive findings in lymph nodes caused by benign reactive lymphocyte proliferation (Troost et al., 2007). The main indication for FLT-PET is therefore prospective assessment of disease response and identification of rapidly proliferating tumor subvolumes, rather than staging.

3.2.1.3. *F-MISO-PET/CT*. Because tumor cell hypoxia is a well-known cause of resistance to treatment, several PET tracers for hypoxia imaging have been developed and tested. These include mainly derivatives of 2-nitroimidazole, such as ^{18}F-fluoro-misonidazole (FMISO) and ^{18}F-Fluoroazomycin arabinoside.

In a study using FMISO-PET, 45 head and neck cancer patients were assessed for tumor hypoxia before treatment. These patients were then treated with radiotherapy and chemotherapy with or without the cytotoxin tirapazamine. The study found that in the hypoxic subpopulation the number of recurrences was significantly decreased if treatment included tirapazamine (Rischin et al., 2006). Importantly, a separate phase II trial that investigated the additive value of tirapazamine in a non-stratified head and neck cancer population failed to show a benefit from tirapazamine (Rischin et al., 2010). These studies illustrate two important considerations for stratifying patient populations by molecular imaging: 1) Novel molecular imaging techniques (such as hypoxia imaging) can be used to identify the proper treatment for patients whose tumors exhibit particular biological characteristics; and 2) without such molecular imaging techniques, the development of an effective treatment regimen could be abandoned due to the absence of proper patient selection.

3.2.1.4. *MRSI*. MRSI of ^{31}P has been shown to enable prediction of tumor grade and therapy response. Cancer typically has elevated resonances corresponding to the phosphomonoester (PME) or phosphodiester (PDE) region of the spectrum.

The PME peak contains phosphocholine (PC). The phosphodiester peak is comprised of glycerol phosphoethanolamone (and glycerol phosphocholine [GPC]), and in some cancers malignant progression is associated with a switch from GPC to PC (Leach et al., 1998; Nelson et al., 2010; Smith et al., 1991). In patients with soft tissue sarcomas, high PME/PDE ratios predicted early response to chemotherapy (Dewhirst et al., 2005, 1990; Lora-Michiels et al., 2006; Sostman et al., 1990). In patients with non-Hodgkin lymphoma, pretreatment levels of PC were able to predict response to chemotherapy, and when these metabolic data were added to the International Prognostic Index for lymphoma, good responders could be separated from those with poor prognoses with increased power (Nelson et al., 2010; Arias-Mendoza et al., 2004, 2006).

3.2.1.5. *Hyperpolarized MRI*. Hyperpolarized [1-^{13}C]pyruvate has shown great promise in preclinical studies for early response assessment (Kurhanewicz et al., 2011). For example, in lymphoma-bearing mice injected with hyperpolarized [1-^{13}C]pyruvate, the LDH-catalyzed interconversion of the ^{13}C label between pyruvate and lactate was shown to decrease early (within 24 h) after the onset of chemotherapy (etoposide) (Day et al., 2007). This early imaging response correlated to the amount of cell death caused by etoposide (Day et al., 2007). The transfer of this technique to the clinic could allow oncologists to discriminate responders and nonresponders early and switch treatments rapidly. Hyperpolarized [1-^{13}C]pyruvate has also been used to visualize prostate cancer and differentiate the various histologic grades on the basis of lactate levels. This has been studied in transgenic adenocarcinoma of mouse prostates (TRAMP) models with promising results (Albers et al., 2008), and clinical trials are currently underway to develop a method for monitoring the therapeutic response of prostate cancer in humans (Kurhanewicz et al., 2011) (Figure 4).

3.2.2. *Radiotherapy*

3.2.2.1. *FDG-PET/CT*. Tumors, tumor subvolumes or lymph nodes that demonstrate high metabolic activity and therefore represent high-risk lesions can be selectively treated with an increased radiation dose.

Several studies in rectal and lung cancer have shown that FDG-PET allows selective boosting of hypermetabolic areas. For example, in a study of 21 patients with small-cell lung cancer, FDG-PET-based radiation planning for mediastinal lymph nodes changed the radiotherapy field in 5 patients (24%) (van Loon et al., 2008).

In patients with head and neck cancer, the radiation boost dose was markedly elevated and directed at the tumors with the highest FDG-avidity, and the adverse treatment-related effects remained limited (Madani et al., 2007).

3.2.2.2. *FLT-PET/CT*. Repetitive FLT-PET scanning has shown some initial promise in the evaluation of early radiotherapy response (Figure 5). In a study of 10 head and neck cancer patients, rapidly decreasing FLT-PET SUVs were observed during the course of radiotherapy. The decrease in FLT activity was noted to precede the volumetric tumor reduction as assessed by conventional CT. The study also showed that it is feasible to apply selective radiotherapy boosts to tumor subvolumes

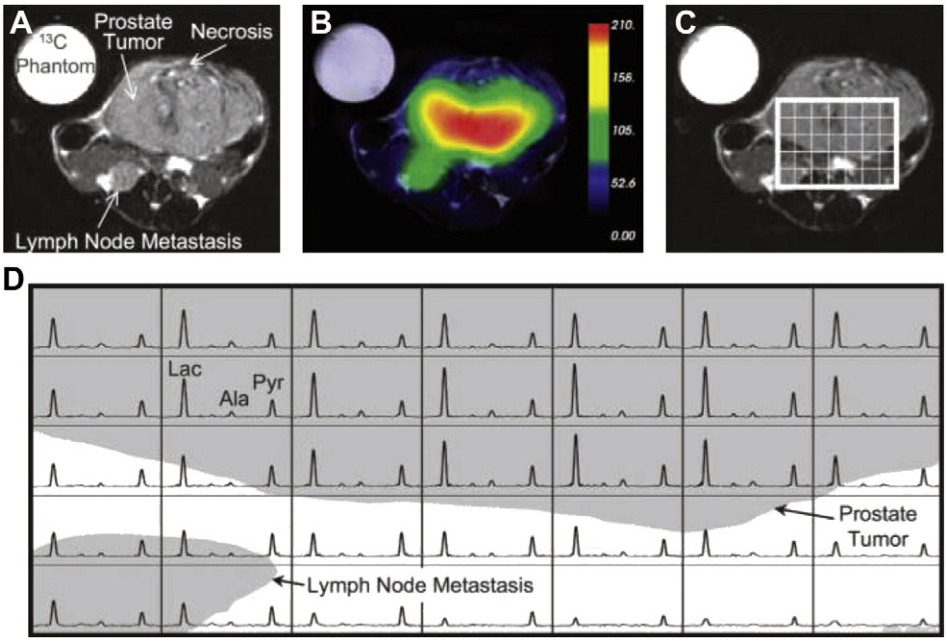

Figure 4 – Axial T_2-weighted ^{1}H image depicting the primary tumor and lymph node metastasis from a TRAMP mouse with a high-grade primary tumor (*A*) and the overlay of an interpolated hyperpolarized ^{13}C lactate image following the injection of 350 μL of hyperpolarized [1-^{13}C]pyruvate (*B*). After spatially zero filling and voxel shifting the ^{13}C spectra to maximize the amount of tumor in the voxels, a subset of the spectral grid was selected (*C*) and displayed (*D*). The three-dimensional MRSI was acquired with a nominal voxel resolution of 135 mm^3 and zero filled to a resolution of 17 mm^3. The spectra show substantially elevated lactate in the high-grade primary tumor. In addition, the metabolite signal is significantly lower in the necrotic regions of the primary tumor. *Lac*, lactate; *Ala*, alanine; *Pyr*, pyruvate. (Reprinted, with permission, from reference (Albers et al., 2008).

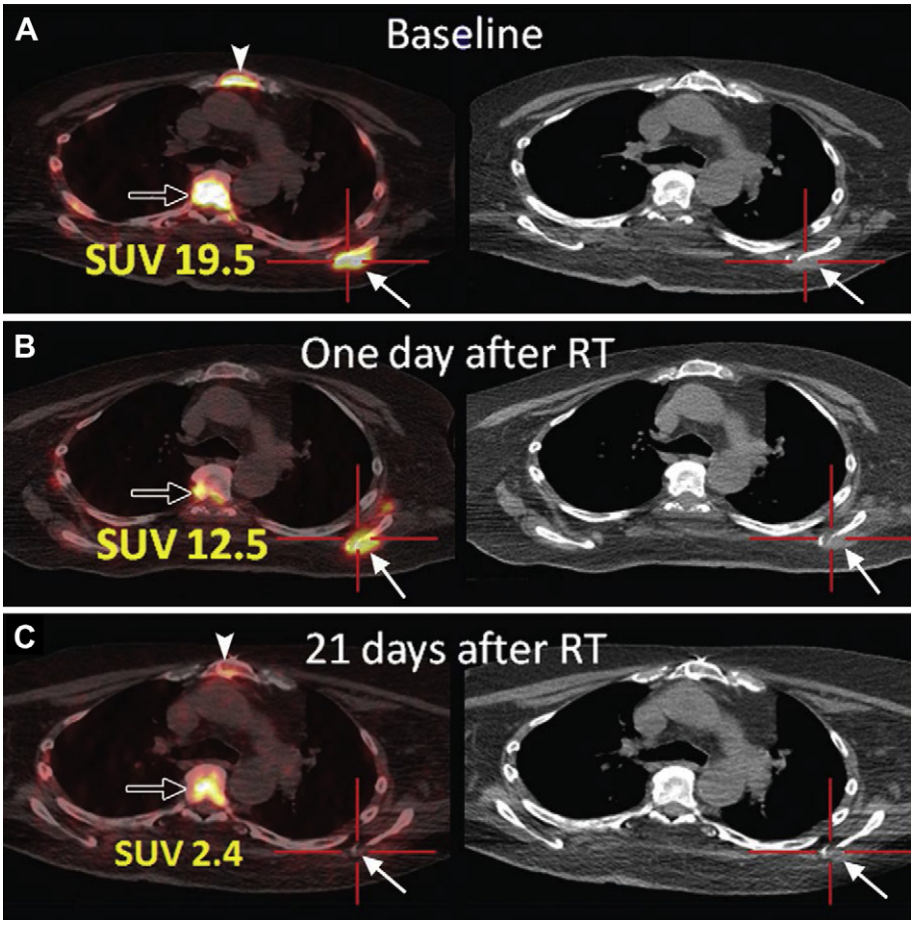

Figure 5 – Images from PET/CT performed by using 18 F L-thymidine (FLT) in a 70-year-old man with widely metastatic squamous cell cancer of the oropharynx. Images were acquired, *A*, before, *B*, 1 day after, and, *C*, 21 days after single dose fraction (2400 cGy) radiation treatment (RT) of a metastatic lesion in the left scapula (solid arrows). There is resolution of uptake at the tumor site in the left scapula. Physiologic FLT uptake is seen in bone marrow of the thoracic spine (open arrow) and sternum (arrowhead). SUV = standardized uptake value. (Reprinted from Hricak H. Oncologic imaging: a guiding hand of personalized cancer care. Radiology. 2011 Jun; 259(3):633–640).

with high FLT activity and therefore to selectively treat tumor areas with high proliferative rates (Troost et al., 2010). However, randomized trials will be needed to assess the improvement in outcome achieved with PET-based radiotherapy.

3.2.2.3. *MRSI*. In organs where the accuracy of PET/CT is limited, MRSI may provide an alternative means for guiding radiotherapy based on molecular information. For example, in a study of patients with glioblastoma multiforme, the presence of metabolic abnormalities consistent with tumor outside of the target volume of Gamma knife radiosurgery predicted significantly shorter survival than their absence (Chan et al., 2004; Graves et al., 2000). Importantly, the study also showed that frequently the new onset of gadolinium enhancement within the target volume was caused by the radiation. This contrast enhancement would have been erroneously interpreted as tumor recurrence without the help of MRSI, which was able to correctly classify it as tumor necrosis.

3.2.3. *Surgery*

Earlier detection of cancer by improved screening methods is expected to increase the importance of curative surgical approaches performed either via open surgery or minimally invasive endoscopic or robotic approaches. Several molecular imaging approaches have been developed for intraoperative guidance, and most of these are based on optical imaging.

One of the first 'enhanced optical imaging' procedures was reported by Haglund et al. in 1996 to identify primary brain tumors using indocyanine green (ICG) (Haglund et al., 1996). In this approach, tumor delineation is based on the principle that ICG clears from solid tumors such as gliomas at a slightly different rate than it clears from the normal brain parenchyma, and that it therefore aggregates disproportionally in tumor tissue (Haglund et al., 1996; Colen et al., 2010). Another approach uses 5-aminolevulenic acid (ALA) to fluorescently label brain tumors. In contrast to ICG, which leaks into the tumor from the disrupted blood–brain barrier, 5-ALA induces intratumoral synthesis of protoporphyrin IX, which is fluorescent. In 2008, Stummer et al. demonstrated that optical imaging with 5-ALA could be used to obtain more complete tumor resection (Stummer et al., 2008). In a theranostic approach, the capability of 5-ALA to fluoresce when excited has been used to develop a robotic laser ablation system. The laser induces ALA fluorescence to allow tumor ablation via laser

photocoagulation (Liao et al., 2008). Intraoperative imaging systems have also been developed for visualization of sentinel lymph node mapping in breast cancer patients using ICG as a near infrared fluorescent lymphatic tracer (Troyan et al., 2009). A dual-modality arginylglycylaspartic acid RGD-coated fluorescent-PET silica nanoparticle has been developed and has been shown to enable improved detection of lymph node metastases in a mini-swine melanoma model (Benezra et al., 2011). The first clinical trial of this nanoparticle in humans was recently initiated at Memorial Sloan-Kettering Cancer Center to evaluate its use with hand-held fluorescent and PET camera systems. Novel multimodality nanoparticle probes (Kircher et al., 2002, 2004) hold promise for combining preoperative MRI with intraoperative optical imaging via a single contrast agent injection (Kircher et al., 2003b). In mouse glioma models, a triple modality MRI-photoacoustic-Raman nanoparticle has been shown to allow gross tumor resection via photoacoustic imaging and fine margin resection via Raman imaging (Kircher et al., in press).

3.3. *Treatment follow-up/restaging*

3.3.1. *FDG-PET/CT*

Following initial treatment of cancer, many patients are at risk of and will eventually experience recurrence. In the detection and evaluation of post-treatment recurrence, conventional cross-sectional imaging (e.g., CT, US and MRI) and, where appropriate, endoscopy are further limited by post-treatment changes such as scar tissue formation and alteration of normal anatomy by surgical resection or reconstructive surgery. Malignant deposits may coexist with scar tissue, which increases the likelihood of sampling error on biopsy. It is important clinically to identify both residual and recurrent cancer and to stratify patients for salvage therapy. In several cancer types, resection of metastases is performed with curative intent. For example in colorectal cancer, not only liver (Chun and Vauthey, 2007), but also lung (Negri et al., 2004) and ovarian (Rayson et al., 2000) metastases are being resected or treated with ablative interventional radiology techniques such as radiofrequency ablation, cryoablation, chemoembolization or Yttrium-90 microspheres. Not surprisingly, given that it is based on metabolic activity of tissues, FDG-PET has been shown to be more accurate than conventional imaging in detecting residual cancer. Marked changes in disease status have been demonstrated in patients with suspected or proven recurrence of colon cancer (Kalff et al., 2002), head and neck cancer (Connell et al., 2007), NSCLC (Hicks et al., 2001), small-cell lung cancer (Blum et al., 2004), and ovarian carcinoma (Simcock et al., 2006). In addition, PET/CT scanners allow metabolically-guided biopsy and thus can minimize sampling errors when there is a need to confirm the presence of disease pathologically.

3.3.2. *MRSI*

In organs that are difficult to evaluate with PET/CT such as the brain and the prostate, MRSI can be used as an alternative method for assessment of tumor recurrence, relying on an elevated ratio of choline to creatine as a tumor marker. Studies have shown that MRSI is able to discriminate residual or recurrent prostate cancer from benign and necrotic tissue after radiotherapy (Pickett et al., 2004; Roach et al., 2001), cryosurgery (Mueller-Lisse et al., 2001a; Parivar et al., 1996; Parivar and Kurhanewicz, 1998), and hormone deprivation therapy (Mueller-Lisse et al., 2001a, 2001b). Early detection of residual cancer with MRSI may allow early intervention with additional therapy.

4. Molecular imaging in drug development

Oncogenes may drive tumor development, and specific therapeutics such as tyrosine kinase inhibitors or antibodies are active against tumors partly because they bind to the protein product of oncogenes and neutralize its action. It follows that these therapeutics could be converted into molecular imaging probes if they could be labeled. Examples include imatinib, a drug which inhibits cKit and has a remarkable inhibitory effect on gastrointestinal stromal tumor (GIST); dasatinib, which is more broadly active against a variety of tyrosine kinase-based receptors such as platelet-derived growth factor in brain tumors; or trastuzumab against Her-2 in breast cancer. We believe that in the future, many of these drugs will be labeled and used as probes, to show specificity of targeting in individual tumors. Present examples include ^{18}F-dasatinib (for bcr/abl, src tyrosine kinase inhibitors) (Veach et al., 2007); ^{124}I-PUH71 (for HSP90) (Moulick et al., 2011); F(ab′)2-trastuzumab-Ga-68 (for HER2) (Smith-Jones et al., 2004); and ^{18}F-imatinib (for bcr/abl) (Glekas et al., 2011). In addition, molecular imaging of high affinity receptors such as estrogen or androgen receptors can be used to show inhibition of the target by estrogen and androgen receptor inhibitor drugs. Active pathways may also be imaged as a basis for choosing patients who are likely to respond to a particular drug; for example, the deoxyribonucleoside salvage pathway may be imaged with new PET probes such as 1-(2′-deoxy-2′-(18)F-fluoro-beta-D-arabinofuranosyl)cytosine (^{18}F-FAC) (Shu et al., 2010). Antibodies comprise one of the largest growing shares of the market for cancer therapies, and more than $30 billion is spent each year on agents such as bevacizumab, cetuximab, and trastuzumab (Holland et al., 2010) to treat human tumors. Molecular imaging is likely to evolve as a basis for monitoring the likelihood of response to individual antibody drugs in cancer patients.

5. Theranostics

The ultimate goal of personalized medicine is to tailor the therapeutic approach for each patient to the specific diagnostic information gathered on that patient's disease. To date, theranostics has usually been practiced by performing *in vitro* testing followed by *in vivo* therapy based on the *in vitro* test result (a *sequential in vitro diagnostic – in vivo therapeutic* approach). A well-known example of this approach is the use of HER-2 testing of breast cancer tissue before the administration of trastuzumab, which targets the HER2 protein in breast cancer (Hricak, 2011). Revolutionary advances in the technology for *in vitro* diagnostics include nuclear MR (NMR)-based biomarker chips (Gaster et al., 2009) and micro-

NMR devices (Haun et al., 2011) for the analysis of soluble biomarkers and biomarkers on whole cells, respectively. Because these devices, in contrast to currently used detection methods, are based on magnetic labeling and readout, they can analyze multiple biomarkers simultaneously without the need to purify samples before analysis. In addition, they have been shown to provide results much more rapidly (within minutes) (Gaster et al., 2009) and to have higher accuracy than current gold standards (Haun et al., 2011). A step beyond a *sequential in vitro* diagnostic – *in vivo* therapeutic approach would be a *sequential in vivo diagnostic – in vivo therapeutic* strategy. For example, an approach already being applied in patients with castration-resistant metastatic prostate cancer is the use of androgen receptor imaging with FDHT PET/CT for the selection and monitoring of treatment with MDV3100, an androgen receptor antagonist (Scher et al., 2010) (Figure 6); because whole-body molecular imaging is used as the *in vivo* diagnostic component, all lesions in a patient, as well as the entirety of each lesion, can be assessed. This represents a tremendous advantage over *in vitro* diagnostic testing, as not every lesion can be biopsied, and analysis of small biopsy samples can assess neither intratumoral heterogeneity nor phenotypic dedifferentiation over time.

The most elegant theranostic approach would be a *combined in vivo diagnostic – in vivo therapeutic* strategy. Receptor-targeting radiopeptides are being developed as single agents for molecular imaging and treatment of tumors that overexpress peptide receptors. To balance the clinical benefits and risks of radionuclide-based therapy, the biodistribution, dosimetry, and toxicity of the therapeutic agent must be carefully monitored. Imaging with targeted radiopeptides can allow detection of metastases, monitoring of treatment efficacy, and detection of progression or recurrence (Mankoff et al., 2008; de Jong et al., 2009). Similar approaches are also being developed using nanotechnology. Unique properties of nanometer-sized particles can be used to target tumors with high affinity and specificity. Either by relying on the enhanced permeability and retention (EPR) effect or by being linked with ligands such as monoclonal antibodies, peptides, or small molecules, nanoparticles may simultaneously serve as therapeutic and imaging contrast agents. Nanoparticles can also be designed to permit multimodality imaging, for example when a particle with optical properties is also paramagnetic and thus detectable by MRI (Kircher et al., in press) or labeled with a radionuclide that makes it detectable by PET (Benezra et al., 2011; Welch et al., 2009). Polymerized nanoparticle platform technology, which allows nanoparticles to be loaded with different targeting moieties, contrast agents, and therapeutic agents, could allow the development of highly personalized treatment regimens (Li et al., 2002).

Figure 6 – FDHT-PET/CT images in a 69-year-old patient with castrate-resistant metastatic prostate cancer (a) prior to and (b) 4 weeks after treatment with MDV3100, an androgen receptor antagonist. The images show a substantial reduction of FDHT accumulation in widespread bone metastases after 4 weeks of treatment, indicating successful targeting of the androgen receptor by MDV3100. (Reprinted from Hricak H. Oncologic imaging: a guiding hand of personalized cancer care. Radiology. 2011 Jun; 259(3):633–640).

6. Integrated diagnostics – Vision for the future

Molecular imaging and molecular imaging-based theranostics are powerful and rapidly evolving disciplines. They have the potential to play key roles in every aspect of oncologic practice, including early disease detection, diagnosis, staging, personalized treatment, treatment monitoring and follow-up. In some cases, as illustrated in this review, this potential has already become reality. Partly because of the noninvasive nature of molecular imaging, the integration of molecular imaging approaches with other *in vitro* tests will be of great value for advancing cancer care. The goal of integrated diagnostics is to make use of all the information available concerning a particular patient to arrive at the most effective, personalized therapy possible. Ideally, integrated diagnostics would rely entirely on diagnostic methods that operate on the molecular level, as only the molecular underpinnings of cancer, and not simply its morphology, can elucidate its true cause and predict its behavior.

One vision for the future, incorporating existing and emerging technology, could be as follows: During a regular screening examination a drop of blood of a patient is placed on an NMR-based biomarker chip (Gaster et al., 2009). This chip analyzes a wide array of cancer biomarkers within minutes and, with high accuracy, diagnoses either the presence or the absence of cancer. The patient then undergoes whole-body molecular imaging in an integrated MRI-PET unit with MR hyperpolarization capability (hMRI-PET). This identifies the locations of the primary tumor and any metastases while obtaining valuable prognostic and predictive biomarkers from metabolic data. Using this whole-body scan as a guide, a fine-needle biopsy is then obtained from a tumor and analyzed with a micro-NMR analysis device, yielding a diagnosis in less than 1 h with an accuracy higher than that of current gold standards such as immunohistochemistry (Haun et al., 2011). Based on the integration of the blood biomarkers, whole-body imaging results, and biopsy findings, personalized treatment is then selected and initiated. If chemotherapy is given, it is tailored via real-time monitoring of the metabolic response with hMRI-PET. If radiotherapy is given, the radiation field and modulations are optimized based on the hMRI-PET scan. If surgery is performed, multimodal nanoparticles can be utilized to facilitate accurate resection (Benezra et al., 2011; Kircher et al., in press).

Imaging and pathology have long played complementary roles in medicine, and optimal implementation of the above or similar integrated diagnostic paradigms will require close collaborations between these two disciplines.

7. Summary

In summary, molecular imaging will play major roles in three important areas of oncology: 1) as a basis for choosing what treatment is right for an individual patient (personalized medicine); 2) as a tool for guiding targeted therapies such as those that require real-time interventions; and 3) as part of the "toolkit" that will be used to develop and optimize new therapeutics, and to document the effectiveness of new classes of drugs in specific patient populations. Multimodality approaches to molecular imaging will increasingly be emphasized – in both hardware and probe development. Technologic improvements have been swift in all the major areas of categorical imaging, including MRI, CT, and ultrasound, and imaging with radionuclides, fluoroscopy and bioluminescence. To optimize the benefits of using several modalities in a cancer patient, fusion or hybrid imaging will become the rule for clinical assessment in the near future. This trend has already been seen in the replacement of separate PET and CT by hybrid PET/CT technology, and will continue with the establishment of integrated MRI/PET.

REFERENCES

Albers, M.J., Bok, R., Chen, A.P., et al., 2008. Hyperpolarized ^{13}C lactate, pyruvate, and alanine: noninvasive biomarkers for prostate cancer detection and grading. Cancer Res. 68 (20), 8607–8615.

Arias-Mendoza, F., Zakian, K., Schwartz, A., et al., 2004. Methodological standardization for a multi-institutional in vivo trial of localized ^{31}P MR spectroscopy in human cancer research. In vitro and normal volunteer studies. NMR Biomed. 17 (6), 382–391.

Arias-Mendoza, F., Payne, G.S., Zakian, K.L., et al., 2006. In vivo ^{31}P MR spectral patterns and reproducibility in cancer patients studied in a multi-institutional trial. NMR Biomed. 19 (4), 504–512.

Bading, J.R., Shields, A.F., 2008. Imaging of cell proliferation: status and prospects. J. Nucl. Med. 49 (Suppl. 2), 64S–80S.

Benezra, M., Penate-Medina, O., Zanzonico, P.B., et al., 2011. Multimodal silica nanoparticles are effective cancer-targeted probes in a model of human melanoma. J. Clin. Invest. 121 (7), 2768–2780.

Blackledge, M.D., Leach, M.O., Collins, D.J., Koh, D.M., 2011. Computed diffusion-weighted MR imaging may improve tumor detection. Radiology.

Blankenberg, F.G., 2008a. In vivo imaging of apoptosis. Cancer Biol. Ther. 7 (10), 1525–1532.

Blankenberg, F.G., 2008b. Monitoring of treatment-induced apoptosis in oncology with PET and SPECT. Curr. Pharm. Des. 14 (28), 2974–2982.

Blum, R., MacManus, M.P., Rischin, D., Michael, M., Ball, D., Hicks, R.J., 2004. Impact of positron emission tomography on the management of patients with small-cell lung cancer: preliminary experience. Am. J. Clin. Oncol. 27 (2), 164–171.

Bole, K., 2010. UCSF News Center. UCSF Web site. "Watchful Waiting" has a New Set of Eyes. Available at: http://www.ucsf.edu/news/2010/11/5846/new-prostate-cancer-imaging-shows-real-time-tumor-metabolism (accessed on 30.9.11).

Bradbury, M., Hricak, H., 2005. Molecular MR imaging in oncology. Magn. Reson. Imaging Clin. N. Am. 13 (2), 225–240.

Brindle, K.M., Bohndiek, S.E., Gallagher, F.A., Kettunen, M.I., 2011. Tumor imaging using hyperpolarized ^{31}C magnetic resonance spectroscopy. Magn. Reson. Med. 66 (2), 505–519.

Buck, A.K., Herrmann, K., Stargardt, T., Dechow, T., Krause, B.J., Schreyogg, J., 2010. Economic evaluation of PET and PET/CT in oncology: evidence and methodologic approaches. J. Nucl. Med. 51 (3), 401–412.

Bury, T., Dowlati, A., Paulus, P., et al., 1996. Evaluation of the solitary pulmonary nodule by positron emission tomography imaging. Eur. Respir. J. 9 (3), 410–414.

Bussink, J., Kaanders, J.H., van der Graaf, W.T., Oyen, W.J., 2011. PET-CT for radiotherapy treatment planning and response

monitoring in solid tumors. Nat. Rev. Clin. Oncol. 8 (4), 233–242.
Cai, W., Chen, X., 2008. Multimodality molecular imaging of tumor angiogenesis. J. Nucl. Med. 49 (Suppl. 2), 113S–128S.
Cai, W., Niu, G., Chen, X., 2008. Imaging of integrins as biomarkers for tumor angiogenesis. Curr. Pharm. Des. 14 (28), 2943–2973.
Chan, A.A., Lau, A., Pirzkall, A., et al., 2004. Proton magnetic resonance spectroscopy imaging in the evaluation of patients undergoing gamma knife surgery for Grade IV glioma. J. Neurosurg. 101 (3), 467–475.
Chun, Y.S., Vauthey, J.N., 2007. Extending the frontiers of resectability in advanced colorectal cancer. Eur. J. Surg. Oncol. 33 (Suppl. 2), S52–S58.
Colen, R.R., Kekhia, H., Jolesz, F.A., 2010. Multimodality intraoperative MRI for brain tumor surgery. Expert Rev. Neurother. 10 (10), 1545–1558.
Connell, C.A., Corry, J., Milner, A.D., et al., 2007. Clinical impact of, and prognostic stratification by, F-18 FDG PET/CT in head and neck mucosal squamous cell carcinoma. Head Neck 29 (11), 986–995.
Conti, P.S., Bading, J.R., Mouton, P.P., Links, J.M., Alauddin, M.M., Fissekis, J.D., et al., 2008. In vivo measurement of cell proliferation in canine brain tumor using C-11-labeled FMAU and PET. Nucl. Med. Biol. 35 (1), 131–141.
Day, S.E., Kettunen, M.I., Gallagher, F.A., et al., 2007. Detecting tumor response to treatment using hyperpolarized ^{13}C magnetic resonance imaging and spectroscopy. Nat. Med. 13 (11), 1382–1387.
de Jong, M., Breeman, W.A., Kwekkeboom, D.J., Valkema, R., Krenning, E.P., 2009. Tumor imaging and therapy using radiolabeled somatostatin analogues. Acc. Chem. Res. 42 (7), 873–880.
Dewhirst, M.W., Sostman, H.D., Leopold, K.A., et al., 1990. Soft-tissue sarcomas: MR imaging and MR spectroscopy for prognosis and therapy monitoring. Work in progress. Radiology 174 (3 Pt 1), 847–853.
Dewhirst, M.W., Poulson, J.M., Yu, D., et al., 2005. Relation between PO_2, ^{31}P magnetic resonance spectroscopy parameters and treatment outcome in patients with high-grade soft tissue sarcomas treated with thermoradiotherapy. Int. J. Radiat. Oncol. Biol. Phys. 61 (2), 480–491.
Downey, R.J., Akhurst, T., Gonen, M., et al., 2004. Preoperative F-18 fluorodeoxyglucose-positron emission tomography maximal standardized uptake value predicts survival after lung cancer resection. J. Clin. Oncol. 22 (16), 3255–3260.
Everitt, S.R., Hicks, J., Ball, D., Kron, T., Schneider-Kolsky, M., Walter, T., Binns, D., MacManus, M., 2009. Imaging cellular proliferation during chemo-radiotherapy: a pilot study of serial ^{18}F-FLT positron emission tomography/computed tomography imaging for non-small-cell lung cancer. Int. J. Radiat. Oncol. Biol. Phys. 75 (4), 1098–1104.
Fletcher, J.W., Djulbegovic, B., Soares, H.P., et al., 2008. Recommendations on the use of ^{18}F-FDG PET in oncology. J. Nucl. Med. 49 (3), 480–508.
Gallagher, F.A., Kettunen, M.I., Day, S.E., et al., 2008. Magnetic resonance imaging of pH in vivo using hyperpolarized ^{13}C-labelled bicarbonate. Nature 453 (7197), 940–943.
Gaster, R.S., Hall, D.A., Nielsen, C.H., et al., 2009. Matrix-insensitive protein assays push the limits of biosensors in medicine. Nat. Med. 15 (11), 1327–1332.
Gatenby, R.A., Gillies, R.J., 2004. Why do cancers have high aerobic glycolysis? Nat. Rev. Cancer 4 (11), 891–899.
Glekas, A.P., Pillarsetty, N.K., Punzalan, B., Khan, N., Smith-Jones, P., Larson, S.M., 2011. In vivo imaging of Bcr-Abl overexpressing tumors with a radiolabeled imatinib analog as an imaging surrogate for imatinib. J. Nucl. Med. 52 (8), 1301–1307.
Golman, K., Olsson, L.E., Axelsson, O., Mansson, S., Karlsson, M., Petersson, J.S., 2003. Molecular imaging using hyperpolarized ^{13}C. Br. J. Radiol. 76 (2), S118–S127.
Grassi, R., Lagalla, R., Rotondo, A., 2008. Genomics, proteomics, mems and saif: which role for diagnostic imaging? La Radiolia Med. 113 (6), 775–778.
Graves, E.E., Nelson, S.J., Vigneron, D.B., et al., 2000. A preliminary study of the prognostic value of proton magnetic resonance spectroscopic imaging in gamma knife radiosurgery of recurrent malignant gliomas. Neurosurgery 46 (2), 319–326. Discussion 26–8.
Grimm, J., Kircher, M.F., Weissleder, R., 2007. Cell tracking. Principles and applications. Radiologe 47 (1), 25–33.
Gupta, N., Gill, H., Graeber, G., Bishop, H., Hurst, J., Stephens, T., 1998. Dynamic positron emission tomography with F-18 fluorodeoxyglucose imaging in differentiation of benign from malignant lung/mediastinal lesions. Chest 114 (4), 1105–1111.
Haglund, M.M., Berger, M.S., Hochman, D.W., 1996. Enhanced optical imaging of human gliomas and tumor margins. Neurosurgery 38 (2), 308–317.
Haun, J.B., Castro, C.M., Wang, R., et al., 2011. Micro-NMR for rapid molecular analysis of human tumor samples. Sci. Transl. Med. 3 (71), 71ra16.
Herrmann, K., Wieder, H.A., Buck, A.K., et al., 2007. Early response assessment using 3'-deoxy-3'-[^{18}F]fluorothymidine-positron emission tomography in high-grade non-Hodgkin's lymphoma. Clin. Cancer Res. 13 (12), 3552–3558.
Hicks, R.J., Kalff, V., MacManus, M.P., et al., 2001. The utility of (18) F-FDG PET for suspected recurrent non-small cell lung cancer after potentially curative therapy: impact on management and prognostic stratification. J. Nucl. Med. 42 (11), 1605–1613.
Holland, J.P., Caldas-Lopes, E., Divilov, V., et al., 2010. Measuring the pharmacodynamic effects of a novel Hsp90 inhibitor on HER2/neu expression in mice using Zr-DFO-trastuzumab. PLoS One 5 (1), e8859.
Howe, F.A., Maxwell, R.J., Saunders, D.E., Brown, M.M., Griffiths, J.R., 1993. Proton spectroscopy in vivo. Magn. Reson. Q. 9, 31–59.
Hricak, H., 2011. Oncologic imaging: a guiding hand of personalized cancer care. Radiology 259 (3), 633–640.
Juweid, M.E., Cheson, B.D., 2006. Positron-emission tomography and assessment of cancer therapy. N. Engl. J. Med. 354 (5), 496–507.
Juweid, M.E., Stroobants, S., Hoekstra, O.S., et al., 2007. Use of positron emission tomography for response assessment of lymphoma: consensus of the Imaging Subcommittee of International Harmonization Project in Lymphoma. J. Clin. Oncol. 25 (5), 571–578.
Kaanders, J.H., Bussink, J., van der Kogel, A.J., 2002. ARCON: a novel biology-based approach in radiotherapy. Lancet Oncol. 3 (12), 728–737.
Kalff, V., Hicks, R.J., Ware, R.E., Hogg, A., Binns, D., McKenzie, A.F., 2002. The clinical impact of (18)F-FDG PET in patients with suspected or confirmed recurrence of colorectal cancer: a prospective study. J. Nucl. Med. 43 (4), 492–499.
Kenny, L., Coombes, R.C., Vigushin, D.M., Al-Nahhas, A., Shousha, S., Aboagye, E.O., 2007. Imaging early changes in proliferation at 1 week post chemotherapy: a pilot study in breast cancer patients with 3'-deoxy-3'-[^{18}F]fluorothymidine positron emission tomography. Eur. J. Nucl. Med. Mol. Imaging 34 (9), 1339–1347.
Kircher, M.F., Willmann J.K. Molecular body imaging: MRI, CT and US. Part I - Principles, Radiology, in press-a.
Kircher M.F., Willmann J.K. Molecular body imaging: MRI, CT and US. Part II - Applications. Radiology, in press-b.
Kircher, M.F., Josephson, L., Weissleder, R., 2002. Ratio imaging of enzyme activity using dual wavelength optical reporters. Mol. Imaging 1 (2), 89–95.

Kircher, M.F., Allport, J.R., Graves, E.E., et al., 2003a. In vivo high resolution three-dimensional imaging of antigen-specific cytotoxic T-lymphocyte trafficking to tumors. Cancer Res. 63 (20), 6838–6846.

Kircher, M.F., Mahmood, U., King, R.S., Weissleder, R., Josephson, L., 2003b. A multimodal nanoparticle for preoperative magnetic resonance imaging and intraoperative optical brain tumor delineation. Cancer Res. 63 (23), 8122–8125.

Kircher, M.F., Weissleder, R., Josephson, L., 2004. A dual fluorochrome probe for imaging proteases. Bioconjug. Chem. 15 (2), 242–248.

Kircher, M.F., Grimm, J., Swirski, F.K., et al., 2008. Noninvasive in vivo imaging of monocyte trafficking to atherosclerotic lesions. Circulation 117 (3), 388–395.

Kircher, M.F., Gambhir, S.S., Grimm, J., 2011. Noninvasive cell-tracking methods. Nat. Rev. Clin. Oncol. 8 (11), 677–688.

Kircher M.F., De la Zerda A., Jokerst J., et al. A brain tumor molecular imaging strategy using a novel triple-modality nanoparticle. Nat. Med., in press.

Koch, A.M., Reynolds, F., Kircher, M.F., Merkle, H.P., Weissleder, R., Josephson, L., 2003. Uptake and metabolism of a dual fluorochrome Tat-nanoparticle in HeLa cells. Bioconjug. Chem. 14 (6), 1115–1121.

Krohn, K.A., Link, J.M., Mason, R.P., 2008. Molecular imaging of hypoxia. J. Nucl. Med. 49 (Suppl 2.), 129S–148S.

Kurhanewicz, J., Vigneron, D.B., Brindle, K., et al., 2011. Analysis of cancer metabolism by imaging hyperpolarized nuclei: prospects for translation to clinical research. Neoplasia 13 (2), 81–97.

Lardinois, D., Weder, W., Hany, T.F., et al., 2003. Staging of non-small-cell lung cancer with integrated positron-emission tomography and computed tomography. N. Engl. J. Med. 348 (25), 2500–2507.

Leach, M.O., Verrill, M., Glaholm, J., et al., 1998. Measurements of human breast cancer using magnetic resonance spectroscopy: a review of clinical measurements and a report of localized ^{31}P measurements of response to treatment. NMR Biomed. 11 (7), 314–340.

Li, K.C., Guccione, S., Bednarski, M.D., 2002. Combined vascular targeted imaging and therapy: a paradigm for personalized treatment. J. Cell. Biochem. Suppl. 39, 65–71.

Liao, H., Shimaya, K., Wang, K., et al., 2008. Combination of intraoperative 5-aminolevulinic acid-induced fluorescence and 3-D MR imaging for guidance of robotic laser ablation for precision neurosurgery. Med. Image Comput. Comput. Assist. Interv. 11 (2), 373–380.

Lora-Michiels, M., Yu, D., Sanders, L., et al., 2006. Extracellular pH and P-31 magnetic resonance spectroscopic variables are related to outcome in canine soft tissue sarcomas treated with thermoradiotherapy. Clin. Cancer Res. 12 (19), 5733–5740.

Lordick, F., Ott, K., Krause, B.J., et al., 2007. PET to assess early metabolic response and to guide treatment of adenocarcinoma of the oesophagogastric junction: the MUNICON phase II trial. Lancet Oncol. 8 (9), 797–805.

Macheda, M.L., Rogers, S., Best, J.D., 2005. Molecular and cellular regulation of glucose transporter (GLUT) proteins in cancer. J. Cell Physiol. 202 (3), 654–662.

Madani, I., Duthoy, W., Derie, C., et al., 2007. Positron emission tomography-guided, focal-dose escalation using intensity-modulated radiotherapy for head and neck cancer. Int. J. Radiat. Oncol. Biol. Phys. 68 (1), 126–135.

Majumder, P.K., Febbo, P.G., Bikoff, R., et al., 2004. mTOR inhibition reverses Akt-dependent prostate intraepithelial neoplasia through regulation of apoptotic and HIF-1-dependent pathways. Nat. Med. 10 (6), 594–601.

Mandrekar, S.J., Sargent, D.J., 2010. Predictive biomarker validation in practice: lessons from real trials. Clin. Trials 7 (5), 567–573.

Mankoff, D.A., Link, J.M., Linden, H.M., Sundararajan, L., Krohn, K.A., 2008. Tumor receptor imaging. J. Nucl. Med. 49 (Suppl. 2), 149S–163S.

Moulick, K., Ahn, J.H., Zong, H., et al., 2011. Affinity-based proteomics reveal cancer-specific networks coordinated by Hsp90. Nat. Chem. Biol..

Mueller-Lisse, U.G., Vigneron, D.B., Hricak, H., et al., 2001a. Localized prostate cancer: effect of hormone deprivation therapy measured by using combined three-dimensional ^{1}H MR spectroscopy and MR imaging: clinicopathologic case-controlled study. Radiology 221 (2), 380–390.

Mueller-Lisse, U.G., Swanson, M.G., Vigneron, D.B., et al., 2001b. Time-dependent effects of hormone-deprivation therapy on prostate metabolism as detected by combined magnetic resonance imaging and 3D magnetic resonance spectroscopic imaging. Magn. Reson. Med. 46 (1), 49–57.

Negri, F., Musolino, A., Cunningham, D., Pastorino, U., Ladas, G., Norman, A.R., 2004. Retrospective study of resection of pulmonary metastases in patients with advanced colorectal cancer: the development of a preoperative chemotherapy strategy. Clin. Colorectal Cancer 4 (2), 101–106.

Nelson, S.J., Kurhanewicz, J., Vigneron, D.B., 2010. Magnetic resonance spectroscopy treatment response and detection. In: Weissleder, R., Ross, B.D., Rehemtulla, A., Gambhir, S.S. (Eds.), Molecular Imaging - Principles and Practice, first ed. People's Medical Publishing House, Shelton, CT, pp. 896–911. USA.

Ohno, Y., Koyama, H., Onishi, Y., et al., 2008. Non-small cell lung cancer: whole-body MR examination for M-stage assessment–utility for whole-body diffusion-weighted imaging compared with integrated FDG PET/CT. Radiology 248 (2), 643–654.

Padhani, A.R., Leach, M.O., 2005. Antivascular cancer treatments: functional assessments by dynamic contrast-enhanced magnetic resonance imaging. Abdom. Imaging 30 (3), 324–341.

Parivar, F., Kurhanewicz, J., 1998. Detection of recurrent prostate cancer after cryosurgery. Curr. Opin. Urol. 8 (2), 83–86.

Parivar, F., Hricak, H., Shinohara, K., et al., 1996. Detection of locally recurrent prostate cancer after cryosurgery: evaluation by transrectal ultrasound, magnetic resonance imaging, and three-dimensional proton magnetic resonance spectroscopy. Urology 48 (4), 594–599.

Patz Jr., E.F., Connolly, J., Herndon, J., 2000. Prognostic value of thoracic FDG PET imaging after treatment for non-small cell lung cancer. AJR Am. J. Roentgenol. 174 (3), 769–774.

Peterson, L.M., Mankoff, D.A., Lawton, T., Yagle, K., Schubert, E.K., Stekhova, S., Gown, A., Link, J.M., Tewson, T., Krohn, K.A., 2008. Quantitative imaging of estrogen receptor expression in breast cancer with PET and 18F-fluoroestradiol. J. Nucl. Med. 49 (3), 367–374.

Pickett, B., Kurhanewicz, J., Coakley, F., Shinohara, K., Fein, B., Roach 3rd, M., 2004. Use of MRI and spectroscopy in evaluation of external beam radiotherapy for prostate cancer. Int. J. Radiat. Oncol. Biol. Phys. 60 (4), 1047–1055.

Pieterman, R.M., van Putten, J.W., Meuzelaar, J.J., et al., 2000. Preoperative staging of non-small-cell lung cancer with positron-emission tomography. N. Engl. J. Med. 343 (4), 254–261.

Pio, B.S., Park, C.K., Pietras, R., et al., 2006. Usefulness of 3'-[F-18] fluoro-3'-deoxythymidine with positron emission tomography in predicting breast cancer response to therapy. Mol. Imaging Biol. 8 (1), 36–42.

Plathow, C., Weber, W.A., 2008. Tumor cell metabolism imaging. J. Nucl. Med. 49 (Suppl. 2), 43S–63S.

Rasey, J.S., Grierson, J.R., Wiens, L.W., Kolb, P.D., Schwartz, J.L., 2002. Validation of FLT uptake as a measure of thymidine kinase-1 activity in A549 carcinoma cells. J. Nucl. Med. 43 (9), 1210–1217.

Rayson, D., Bouttell, E., Whiston, F., Stitt, L., 2000. Outcome after ovarian/adnexal metastectomy in metastatic colorectal carcinoma. J. Surg. Oncol. 75 (3), 186–192.

Rischin, D., Hicks, R.J., Fisher, R., et al., 2006. Prognostic significance of [^{18}F]-misonidazole positron emission tomography-detected tumor hypoxia in patients with advanced head and neck cancer randomly assigned to chemoradiation with or without tirapazamine: a substudy of Trans-Tasman Radiation Oncology Group Study 98.02. J. Clin. Oncol. 24 (13), 2098–2104.

Rischin, D., Peters, L.J., O'Sullivan, B., et al., 2010. Tirapazamine, cisplatin, and radiation versus cisplatin and radiation for advanced squamous cell carcinoma of the head and neck (TROG 02.02, HeadSTART): a phase III trial of the Trans-Tasman Radiation Oncology Group. J. Clin. Oncol. 28 (18), 2989–2995.

Roach 3rd, M., Kurhanewicz, J., Carroll, P., 2001. Spectroscopy in prostate cancer: hope or hype? Oncol. (Williston Park) 15 (11), 1399–1410 Discussion 415-6, 418.

Sachs, S., Bilfinger, T.V., 2005. The impact of positron emission tomography on clinical decision making in a university-based multidisciplinary lung cancer practice. Chest 128 (2), 698–703.

Scher, H.I., Beer, T.M., Higano, C.S., et al., 2010. Antitumour activity of MDV3100 in castration-resistant prostate cancer: a phase 1–2 study. Lancet 375 (9724), 1437–1446.

Schiepers, C., Dahlbom, M., Chen, W., et al., 2010. Kinetics of 3'-deoxy-3'-^{18}F-fluorothymidine during treatment monitoring of recurrent high-grade glioma. J. Nucl. Med. 51 (5), 720–727.

Seam, P., Juweid, M.E., Cheson, B.D., 2007. The role of FDG-PET scans in patients with lymphoma. Blood 110 (10), 3507–3516.

Shields, A.F., Grierson, J.R., Dohmen, B.M., et al., 1998. Imaging proliferation in vivo with [F-18]FLT and positron emission tomography. Nat. Med. 4 (11), 1334–1336.

Shu, C.J., Campbell, D.O., Lee, J.T., et al., 2010. Novel PET probes specific for deoxycytidine kinase. J. Nucl. Med. 51 (7), 1092–1098.

Simcock, B., Neesham, D., Quinn, M., Drummond, E., Milner, A., Hicks, R.J., 2006. The impact of PET/CT in the management of recurrent ovarian cancer. Gynecol. Oncol. 103 (1), 271–276.

Smith, T.A., Glaholm, J., Leach, M.O., et al., 1991. A comparison of in vivo and in vitro ^{31}P NMR spectra from human breast tumours: variations in phospholipid metabolism. Br. J. Cancer 63 (4), 514–516.

Smith-Jones, P.M., Solit, D.B., Akhurst, T., Afroze, F., Rosen, N., Larson, S.M., 2004. Imaging the pharmacodynamics of HER2 degradation in response to Hsp90 inhibitors. Nat. Biotechnol. 22 (6), 701–706.

Sostman, H.D., Charles, H.C., Rockwell, S., et al., 1990. Soft-tissue sarcomas: detection of metabolic heterogeneity with P-31 MR spectroscopy. Radiology 176 (3), 837–843.

Strauss, H.W., Blankenberg, F., Vanderheyden, J.L., Tait, J., 2008. Translational imaging: imaging of apoptosis. Handbook Exp. Pharmacol. 185 (Pt 2), 259–275.

Stummer, W., Reulen, H.J., Meinel, T., et al., 2008. Extent of resection and survival in glioblastoma multiforme: identification of and adjustment for bias. Neurosurgery 62 (3), 564–576. Discussion -76.

Swirski, F.K., Pittet, M.J., Kircher, M.F., et al., 2006. Monocyte accumulation in mouse atherogenesis is progressive and proportional to extent of disease. Proc. Natl. Acad. Sci. USA 103 (27), 10340–10345.

Troost, E.G., Vogel, W.V., Merkx, M.A., et al., 2007. ^{18}F-FLT PET does not discriminate between reactive and metastatic lymph nodes in primary head and neck cancer patients. J. Nucl. Med. 48 (5), 726–735.

Troost, E.G., Bussink, J., Slootweg, P.J., et al., 2010. Histopathologic validation of 3'-deoxy-3'-^{18}F-fluorothymidine PET in squamous cell carcinoma of the oral cavity. J. Nucl. Med. 51 (5), 713–719.

Troyan, S.L., Kianzad, V., Gibbs-Strauss, S.L., et al., 2009. The FLARE intraoperative near-infrared fluorescence imaging system: a first-in-human clinical trial in breast cancer sentinel lymph node mapping. Ann. Surg. Oncol. 16 (10), 2943–2952.

van Loon, J., Offermann, C., Bosmans, G., et al., 2008. 18FDG-PET based radiation planning of mediastinal lymph nodes in limited disease small cell lung cancer changes radiotherapy fields: a planning study. Radiother. Oncol. 87 (1), 49–54.

van Ufford, H.M., Kwee, T.C., Beek, F.J., et al., 2011. Newly diagnosed lymphoma: initial results with whole-body T1-weighted, STIR, and diffusion-weighted MRI compared with ^{18}F-FDG PET/CT. AJR Am. J. Roentgenol. 196 (3), 662–669.

Veach, D.R., Namavari, M., Pillarsetty, N., et al., 2007. Synthesis and biological evaluation of a fluorine-18 derivative of dasatinib. J. Med. Chem. 50 (23), 5853–5857.

Viale, A., Aime, S., 2010. Current concepts on hyperpolarized molecules in MRI. Curr. Opin. Chem. Biol. 14 (1), 90–96.

von Schulthess, G.K., Steinert, H.C., Hany, T.F., 2006. Integrated PET/CT: current applications and future directions. Radiology 238 (2), 405–422.

Warburg, O., Wind, F., Negelein, E., 1927. The metabolism of tumors in the body. J. Gen. Physiol. 8 (6), 519–530.

Weber, G., 1977a. Enzymology of cancer cells (second of two parts). N. Engl. J. Med. 296 (10), 541–551.

Weber, G., 1977b. Enzymology of cancer cells (first of two parts). N. Engl. J. Med. 296 (9), 486–492.

Weber, W.A., 2006. Positron emission tomography as an imaging biomarker. J. Clin. Oncol. 24 (20), 3282–3292.

Weissleder, R., Pittet, M.J., 2008. Imaging in the era of molecular oncology. Nature 452 (7187), 580–589.

Welch, M.J., Hawker, C.J., Wooley, K.L., 2009. The advantages of nanoparticles for PET. J. Nucl. Med. 50 (11), 1743–1746.

Westphalen, A.C., McKenna, D.A., Kurhanewicz, J., Coakley, F.V., 2008. Role of magnetic resonance imaging and magnetic resonance spectroscopic imaging before and after radiotherapy for prostate cancer. J. Endourol. 22 (4), 789–794.

W N, 1992. Studies of human tumors by MRS: a review. NMR Biomed. 5 (5), 303–324.

Zakian, K.L., Hricak, H., Ishill, N., et al., 2010. An exploratory study of endorectal magnetic resonance imaging and spectroscopy of the prostate as preoperative predictive biomarkers of biochemical relapse after radical prostatectomy. J. Urol. 184 (6), 2320–2327.

Zavaleta, C.L., Kircher, M.F., Gambhir, S.S., 2011. Raman's "effect" on molecular imaging. J. Nucl. Med. 52 (12), 1839–1844.

Zhao, M., Kircher, M.F., Josephson, L., Weissleder, R., 2002. Differential conjugation of tat peptide to superparamagnetic nanoparticles and its effect on cellular uptake. Bioconjug. Chem. 13 (4), 840–844.